Processing of tissue sensing adaptive radar data - an analogue for georadar

Adrian D. Smith, Jérémie Bourqui*, Yuhong (Kay) Liu*, Elise C. Fear*, Robert J. Ferguson

ABSTRACT

Frequency domain georadar data have several advantages over time domain data but are much more cumbersome to acquire. A medical imaging technique developed in the Department of Electrical Engineering at the University of Calgary known as "tissue sensing adaptive radar" (TSAR) makes use of monostatic radar data acquired in the frequency domain. Simulated data were generated and processed using a workflow that has been previously developed and implemented sucessfully on georadar data. We discover that the simulated TSAR data are mixed phase, violating the minimum-phase assumptions of deconvolution. We show through synthetic examples that deconvolution of these data does not recover reflectivity accurately. Although nonstationary Gabor deconvolution has been shown be effective when applied to georadar data, our work with the TSAR data shows that we must take care to ensure that radar data be minimum phase during deconvolution, especially with data acquired in the frequency domain.

INTRODUCTION

Many fields, including the earth sciences and medical imaging make use of the radar reflection method. The method involves emitting controlled pulses of electromagnetic radiation in the radio to microwave band from an antenna, which reflect off objects in their path (Jol, 2009). Subsequent processing of the backscattered signal generates an image of the region of interest. Analagous to acoustic impedance in seismic, radar reflections result from a change in relative electric permitivity (ε_r) between media. From Davis and Annan (1989), normal incidence reflection coefficients for radar (R) are given by:

$$R = \frac{\sqrt{\varepsilon_{r1}} - \sqrt{\varepsilon_{r2}}}{\sqrt{\varepsilon_{r1}} + \sqrt{\varepsilon_{r2}}} \tag{1}$$

where ε_{r1} and ε_{r2} are the relative electric permittivities of the incident and transmissive media respectively. Assuming a low-loss geological environment, the relative electric permittivity is related to the velocity of electromagnetic radiation in a medium (v) by:

$$v = \frac{c}{\sqrt{\varepsilon_r}} \tag{2}$$

where c is the speed of light in a vaccum ($c \approx 0.3$ m/ns) (Fisher et al., 1992)

*Department of Electrical Engineering, University of Calgary

Georadar

Georadar (also known as ground penetrating radar or GPR), is a geophysical application of the radar reflection method used for exploration in the near-subsurface. It has been used in a number of geological applications (Ferguson et al. (2012a), Rowell et al. (2010), Ferguson et al. (2012b)), as well as archeological and engineering applications (Goodman (1994), Jol (2009)). The majority of georadar data is aqcuired in the time domain, with transmitters and receivers being at common offset (usually fixed to a cart). This is usually done to speed up data acquisition. However, non-fixed recievers can be used to acquire multi-offset data, which can be used for NMO velocity analysis (eg. Fisher et al. (1992)). Additionally, Georadar data can be acquired directly in the frequency domain by using a stepped-frequency continuous-wave (SFCW) system (Garbuz et al. (2009), Yedlin et al. (2010)).

Georadar is analagous to seismic in a number of ways. Both methods involve active controlled sources emitting energy into the subsurface. Receivers record reflected and diffracted energy from physical property changes in the subsurface. Their respective expressions for reflection coefficients are of the same approximate mathematical form (equation 1). Two significant differences between seismic data and georadar data are scale and attenuation. Georadar data deals with much smaller scale units than does seismic data. Spatial units are in m to km (vs. m to km in seismic), temporal units are on the order of magnitude of ns (vs. ms to s in seismic), velocities are given either as a fraction of c m/s or as m/ns (vs. m/s to km/s in seismic), and frequencies are in the MHz to GHz range (vs. Hz for seismic data). Georadar signals also attenuate much more strongly than seismic data. Ferguson and Margrave (2012) determined that the attenuation factor Q is about an order of magnitude lower for georadar than seismic, meaning that the attenuation effect itself is much larger for georadar than for seismic. Attenuation in georadar data is strongly related with the electrical properties of the shallow subsurface. It fares poorly in regions with liquid water in the shallow subsurface, high-conductivity materials such was clay soils, and regions with highly heterogeneous conditions such as rocky soils (Jol, 2009).

As mentioned previously, georadar data can be acquired in both time (impulse) and frequency (SFCW) domains. There are several significant advantages to acquiring frequency domain data however:

- Frequency domain georadar data has greater measurement accuracy because it is much easier to synthesize a pure tone at a given frequency than to measure a time delay.
- SFCW systems have greater dynamic ranges and lower noise thresholds becuase they can transmit higher power than impulse systems.

(Garbuz et al., 2009)

This is of great importance as impulse data is only recorded in 16-bit, and this limited dynamic range results in clipping of stronger amplitude signatures and loss of low amplitude signatures (Gulati, 2011). However, time domain data requires much less time to

acquire and as a result is still preferred in most cases over SFCW frequency domain data (Garbuz et al., 2009).

TISSUE SENSING ADAPATIVE RADAR (TSAR)

Tissue sensing adaptive radar (TSAR) is a prototype alternative diagnostic breast imaging method developed in the Department of Electrical Engineering at the University of Calgary (Bourqui et al., 2012). It is designed to compliment other medical imaging techniques in the detection of breast cancer. The motivation for developing the method is the fact that there are significant contrasts in dielectric properties at microwave frequencies between normal and malignant breast tissue (Fear et al., 2002). Following from this is the idea that a radar reflection method could be developed to record these dielectric contrasts as diffractions and reflections, and eventually generate an image of the breast highlighting the number and location of possible cancerous growths.

The TSAR method uses a monostatic radar approach, whereby a single antenna scans around the breast of the patient as it immersed in a tank containing canola oil (Figure 1). At each scan location, measurements are taken at 1601 points over the frequency range from 50MHz to 15GHz. The process of moving the sensors and collecting measurements takes less than 30 minutes for 1 breast scanned at up to 200 different antenna locations (Bourqui et al., 2012).

The monostatic approach is novel and although it does not collect as much data as its multistatic counterpart, the system can be designed to produce a focused beam, increasing the reflected power from small features (Bourqui et al., 2012). This is beneficial due to the potential for high attenuation in breast tissues. The custom antenna used is a balanced antipodal Vivaldi antenna with a director (BAVA-D), (Bourqui et al., 2010). The director narrows the beam of the antenna compared with a standard BAVA design, thus focusing more energy into the breast and enhancing reflections.

Motivation

TSAR data represents a type of frequency radar data that has similar charcteristics to georadar data. It is ideally suited for testing different processing and imaging workflows that can be eventually applied to field georadar data. Another benefit is a fine enough station interval to avoid spatial aliasing. This will an important factor in future work, as the ulimate goal is to image the dataset in depth.

TSAR DATA SIMULATION

TSAR-like data were simulated using software developed by the Department of Electrical Engineering at the University of Calgary. The simulation space consisted of a two dimensional plane 16cm wide and 8cm deep of homogenous and lossless canola oil ($\varepsilon_r \approx 2.5$), with z corresponding to depth and x corresponding to the axis along which the antenna was moved. Inclusions of higher relative permittivity at unknown locations were added to the simulation, representing imaging targets such as possible tumors (Figure 2). The BAVA-D (Bourqui et al., 2010) antenna was used, directed towards the negative z

direction. Parameters for the aquisition geometry of the simulation are as follows:

Table 1. TSAR Simulation Parameters

Parameter	Value
Sensor Spacing	0.001 cm
Number of Locations	101
Frequency Range	0 - 14.99 GHz
Frequency Step	10 MHz

TSAR PRE-PROCESSING

A number of pre-processing steps were undertaken before any deconlvolution or imaging of the data was attempted. First, the antenna response was removed from the data. The data were with and without inclusions present in the medium. With no inclusions present, the recorded data represents just the antenna repsonse (Figure 3). This is used to remove this noise from the data with inclusions present. The data were then loaded into Octave. For each trace, the data were in the form of a complex number assosciated with a frequency (4). The data were then transferred to the time domain using a band-limited inverse Fourier transfrom (*bltifft*), available in the CREWES Matlab Toolbox.

Determination of Time Correction to $Z = 0$

After converting the data to the time domain, we needed to identify the location in time corresponding to the $z = 0$m depth. In this case we can calbirate the antenna using at least two perfectly electrically conducting (PEC) plates placed at known depths (Figure 6). The plates are designed to generate strong radar reflections due to their dielectric properties. We record the signal with each individual plate in and define the location of each plate in the time domian as the maximum of the envelope of the reflections (Figure 7).

As we know the actual distance between the vertical plates, know the difference in travel times between them, and assume the medium is homogeneous, we can estimate the velocity of the medium v as:

$$v = 2 * \left(\frac{z_2 - z_1}{t_{PEC2} - t_{PEC1}} \right) \tag{3}$$

where z_1 and z_2 are the depths of the two PEC plates with respect to z_0 = 0 m (which in our case are 0.02 and 0.08 m respectively) (Figure 6), and t_{PEC1} and t_{PEC2} are the time domain locations of the envelope peaks from the respective peaks. Using this formulation, the velocity of the medium was calculated to be ≈ 0.191 m/ns. This compares favourably with 0.190 m/ns, which is the calculated radar velocity of canola oil using Equation 2, assuming $\varepsilon_r = 2.5$.

Since we now know the radar velocity of the medium along with the PEC location in distance, we were able to calaculate the location of $z = 0$ in the time domain and the corresponding time shift required to datum the data properly to be 1.4513 ns.

Frequency Filtering

After shifting the TSAR data to the proper datum, a filter was applied to the data in order to remove high frequency noise associated with instrument noise. The amplitude spectra for the TSAR data traces were weighted by the ampitude spectrum of the TSAR pulse used as the source in the simulation (figures 9 and 10). The source tsar pulse has a form of:

$$v(t) = v_0 \cdot (t - t_0) \cdot e^{\frac{-(t-t_0)^2}{\tau^2}}, \tag{4}$$

,

where v_0 is used to adjust the amplitude, $\tau = 62.5ps$ and $t_0 = 4\tau$ (Bourqui et al., 2010).

NONSTATIONARY GABOR DECONVOLUTION

nonstationary deconvolution has been shown previously to be a superior pre-processing flow for radar data (Ferguson et al., 2012a). the nonstationary deconvolution accounts for attentuation in the source wavelet and thus is able to recover substantially more signal at later arrival times. this workflow is based on gabor deconvolution algorithms developed at CREWES.

minimum phase assumption

An excellent overview of Gabor Deconvolution is given by Margrave et al. (2011). One of the major assumptions utilized by this method (and many other types of seismic and radar signal processing methods) is that of minimum phase. Since the TSAR is acquired in the frequency domain and does not necessarily meet this requirement. To demonstrate this, we attempt to construct a minimum-phase version of the TSAR pulse using the methods outlined in Lamoureux and Margrave (2007a), Lamoureux and Margrave (2007c), and Lamoureux and Margrave (2007b). These make use of the *cepstrum* function available in MATLAB. Although our results are preliminary, they show that the TSAR pulse is indeed NOT minimum phase, and this needs to be dealt with for future processing and imaging, especially for deconvolution (Figures 12, 13, and 14).

CONCLUSIONS / FUTURE WORK

TSAR data were sucessfully converted from their raw form into the time domain, datumed and filtered successfully. We wish to pursue nonstationary Gabor deconvolution as our next processing step, however cannot guarantee accurate results due to the mixed phase nature of the TSAR wavelet. This is also of huge significance to other forms of radar, notably georadar. The next step is to develop a method to overcome this limitation, and to evenutally move on to imaging the data and improving the images that we can develop of the breast using this technique.

ACKNOWLEDGEMENTS

we would like to thank crewes and the department of electrical engineering for providing data and matlab code used in this work. additionally, we would like to thank crewes

and crewes sponsors for their support and funding.

REFERENCES

Bourqui, J., Okoniewski, M., and Fear, E. C., 2010, Balanced anitpodal vivaldi antenna with dielectric director for near-field microwave imaging: IEEE Transactions on Biomedical Engineering, **58**, 2318–2326.

Bourqui, J., Sill, J. M., and Fear, E. C., 2012, A prototype system for measuring microwave frequency reflections from the breast: International Journal of Biomedical Imaging, **2012**.

Davis, J. L., and Annan, A. P., 1989, Ground-penetrating radar for high-resolution mapping of soil and rock stratigraphy: Geophysical Prospecting, **37**, 531–551.

Fear, E. C., Li, X., Hagness, S. C., and Stuchly, M. A., 2002, Confocal microwave imaging for breast cancer detection: Localization of tumors in three dimensions: IEEE Transactions on Biomedical Engineering, **49**, No. 8, 812–822.

Ferguson, R. J., Ercoli, M., and Frigeri, A., 2012a, Georadar data processing and imaging: paleoseismicity in the piano di castelluccio basin, central italy: CREWES Research Report, **24**.

Ferguson, R. J., and Margrave, G. F., 2012, Attenuation compensation for georadar data by gabor deconvolution: CREWES Research Report, **24**.

Ferguson, R. J., Y[edin], M. J., C[hristian], Pichot, Dauvignac, J.-Y., Fortino, N., and Gaffet, S., 2012b, Depth migration of monostatic and bistatic georadar data: CREWES Research Report, **24**.

Fisher, S. C., Stewart, R. R., and Jol, H. M., 1992, Processing ground penetrating (gpr) data: CREWES Research Report, **4**, 11.1–11.22.

Garbuz, A. C., McClellan, J. H., and Scott, W. R., 2009, A compressive sensing data acquisition and imaging method for stepped frequency gprs: IEEE Transactions on Signal Processing, **57**, No. 7, 2640–2650.

Goodman, D., 1994, Ground-penetrating radar simulation in engineering and archaeology: Geophysics, **59**, No. 2, 224–232.

Gulati, A., 2011, Fourier reconstruction of signal: M.Sc. thesis, Univ. of Calgary.

Jol, H. M., Ed., 2009, Ground penetrating radar theory and applications: Elsevier Science.

Lamoureux, M. P., and Margrave, G. F., 2007a, An analytic approach to minimum phase signal: CREWES Research Report, **19**.

Lamoureux, M. P., and Margrave, G. F., 2007b, A band-limited minimum phase calculation: CREWES Research Report, **19**.

Lamoureux, M. P., and Margrave, G. F., 2007c, A minimum-phase, band-limited delta spike: CREWES Research Report, **19**.

Margrave, G. F., Lamoureux, M. P., and Henley, D. C., 2011, Gabor deconvolution: Estimating reflectivity by nonstationary deconvolution of seismic data: Geophysics, **76**, No. 3, W15–W30.

Rowell, C. R., Pidlisecky, A., Irving, J. D., and Ferguson, R. J., 2010, Characterization of lava tubes using ground penetrating radar at craters of the moon national monument, usa: CREWES Research Report, **22**.

Yedlin, M., Senechal, G., Rousset, D., Fortino, N., Dauvignac, J. Y., Gaffet, S., Monfret, T., and Pichot, C., 2010, Comparative study using an uwb measurement system and a ramac gpr system for subsurface imaging of the vaucluse karst aquifer, *in* Wireless Information Technology and Systems (ICWITS), 2010 IEEE International Conference on, Honolulu, Hawaii, 1–4.

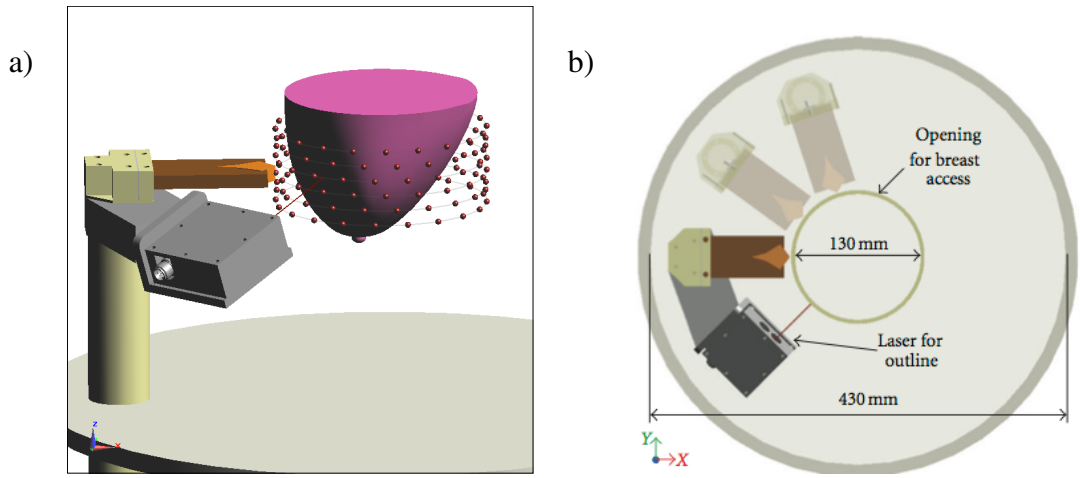

FIG. 1. 3D illustration of the prototype TSAR system. View of the scan pattern used for measurement a). Each sphere corresponds to an antenna location. A plan view of the device is shown in b). The laser is used to determine the distance from the antenna aperture to the irregular surface of the skin on the breast (Bourqui et al., 2012).

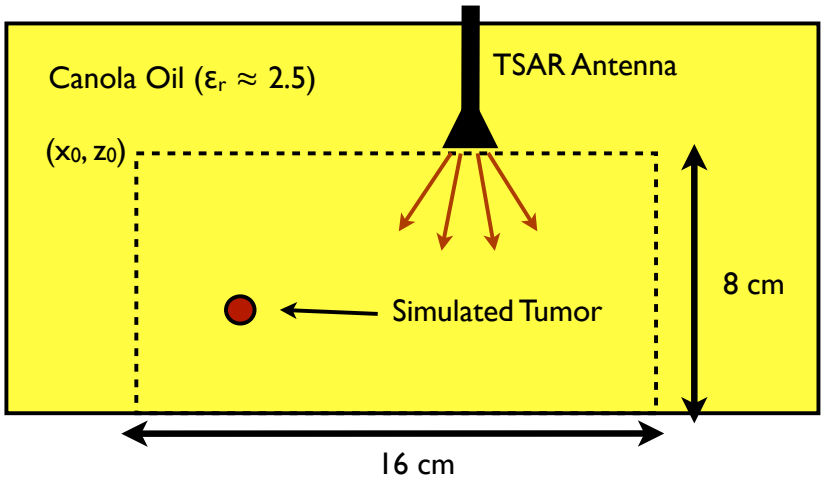

FIG. 2. Schematic of TSAR simulation space. See Table 1 for acquisition parameters.

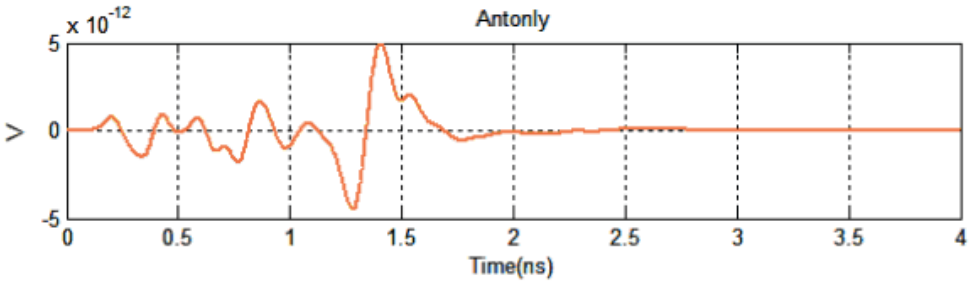

FIG. 3. Illustration of the antenna only response in the TSAR simulation space.

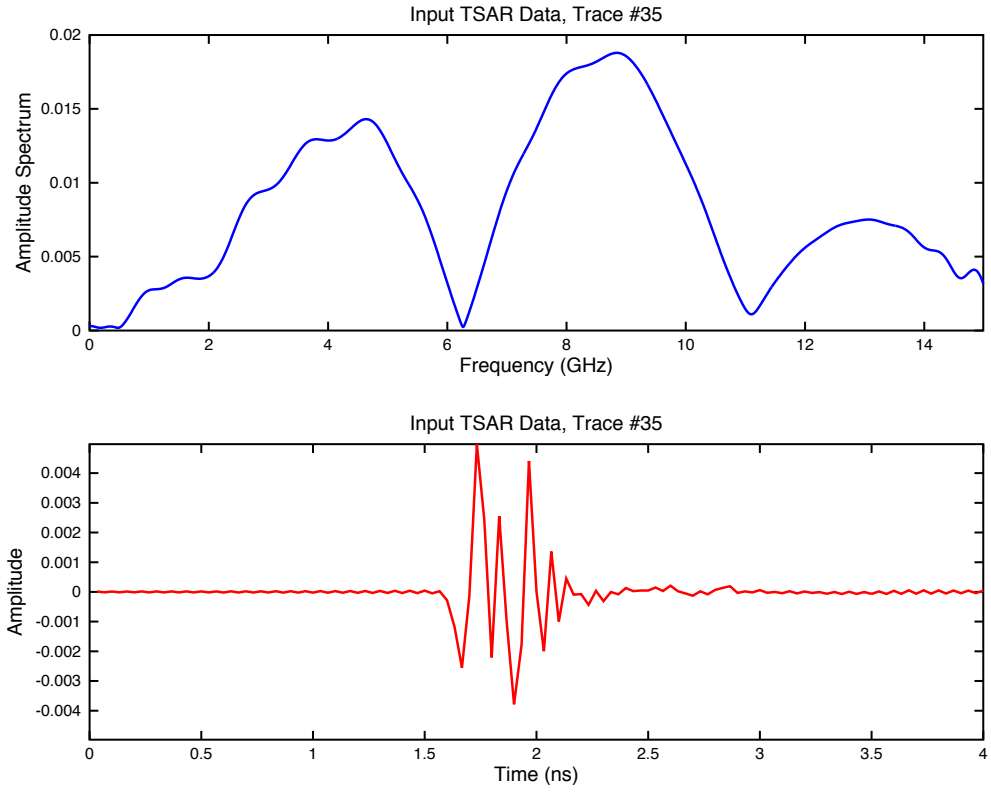

FIG. 4. Raw simulated TSAR data from a single trace, with the upper image representing the raw frequency domain data and the lower image being the time domain reconstruction using *bltifft* from the CREWES toolbox.

a)

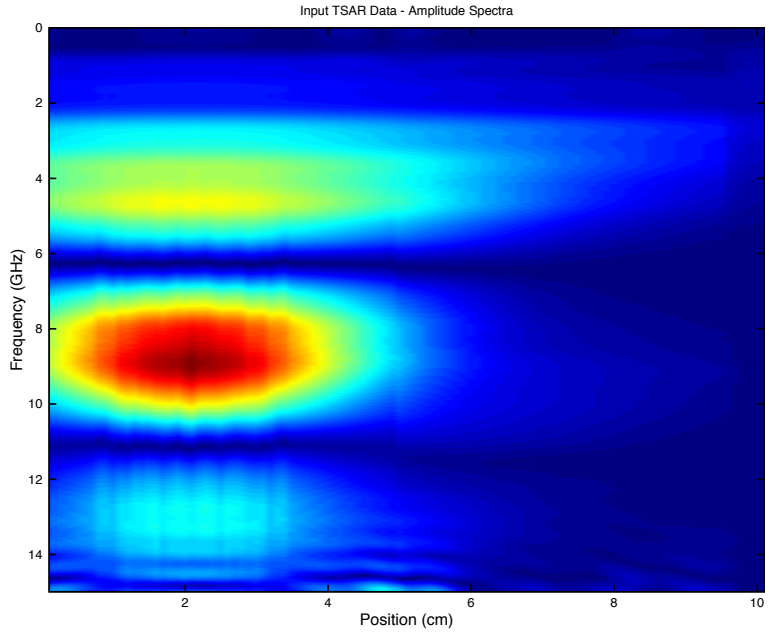

b)

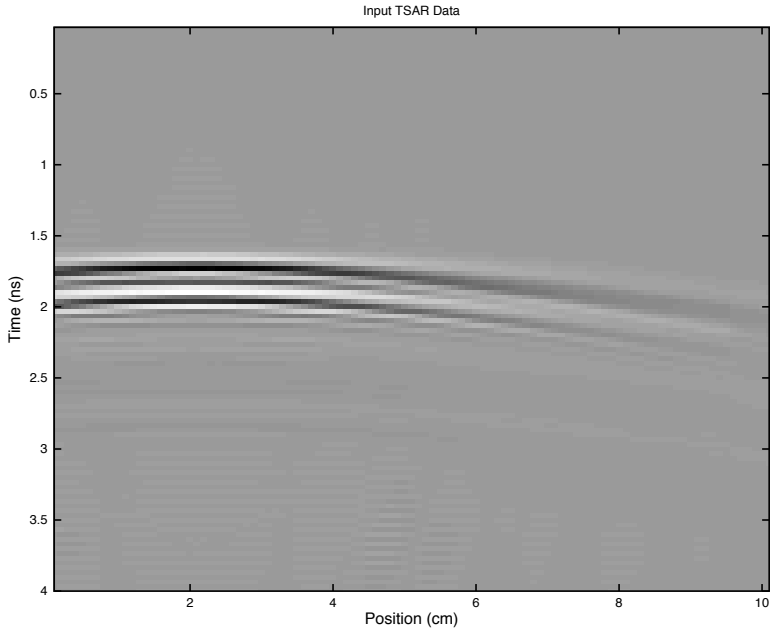

FIG. 5. Raw simulated TSAR data for the entire record. Raw frequency domain data a), and time domain reconstruction using *bltifft* from the CREWES Matlab toolbox.

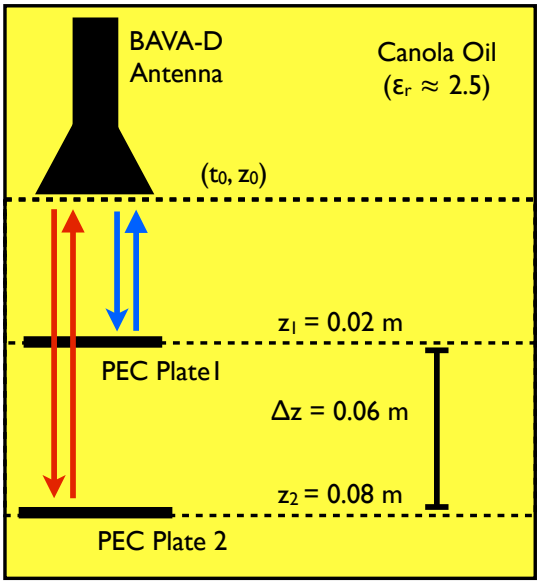

FIG. 6. Schematic illustrating the determination of the $z_0 = 0$ m location in time. Two perfectly electrically conducting (PEC) plates were individually placed in the simulation at known z locations and two-way-traveltimes (TWT) from each reflection recorded. Using this information, the velocity of the medium was estimated, as well as the time shift needed to reposition to $z_0 = 0$ m on the simulation data.

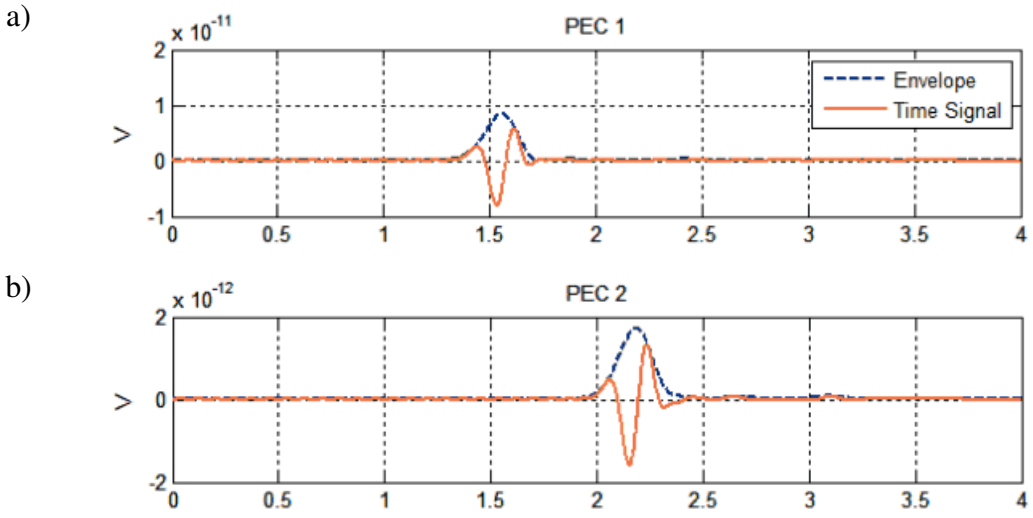

FIG. 7. View of the reflections from the perfectly electrically conducting (PEC) plates located at $z_1 = 0.02$ m a), and $z_2 = 0.06$ m b). The envelope of the PEC reflections are shown with the blue dashed line, and the envelope peaks were used to estimate the time shift required to move $z_0 = 0$ m to zero time. Note that the amplitude of these reflections are much weaker than the signature of the antenna response (Figure 3, illustrating why it must be removed first.

a)

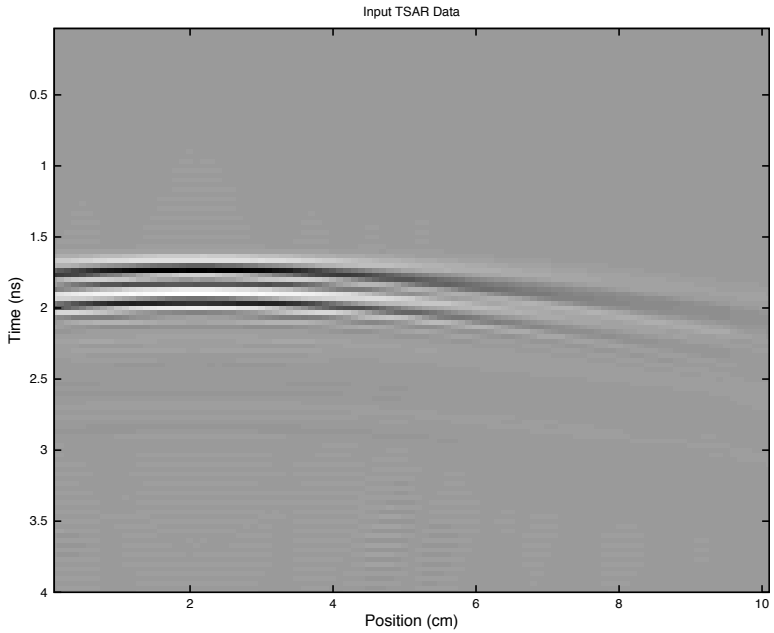

b)

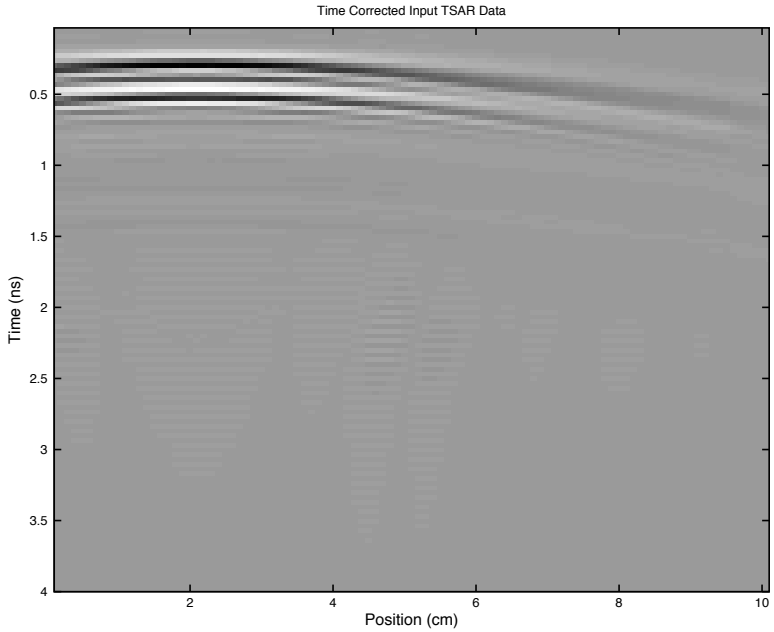

FIG. 8. Reconstructed time domain TSAR data records. Raw input data in a), with time corrected data in b). The data in b) were shifted by the delay calculated using the principles outlined in (Figure 6.)

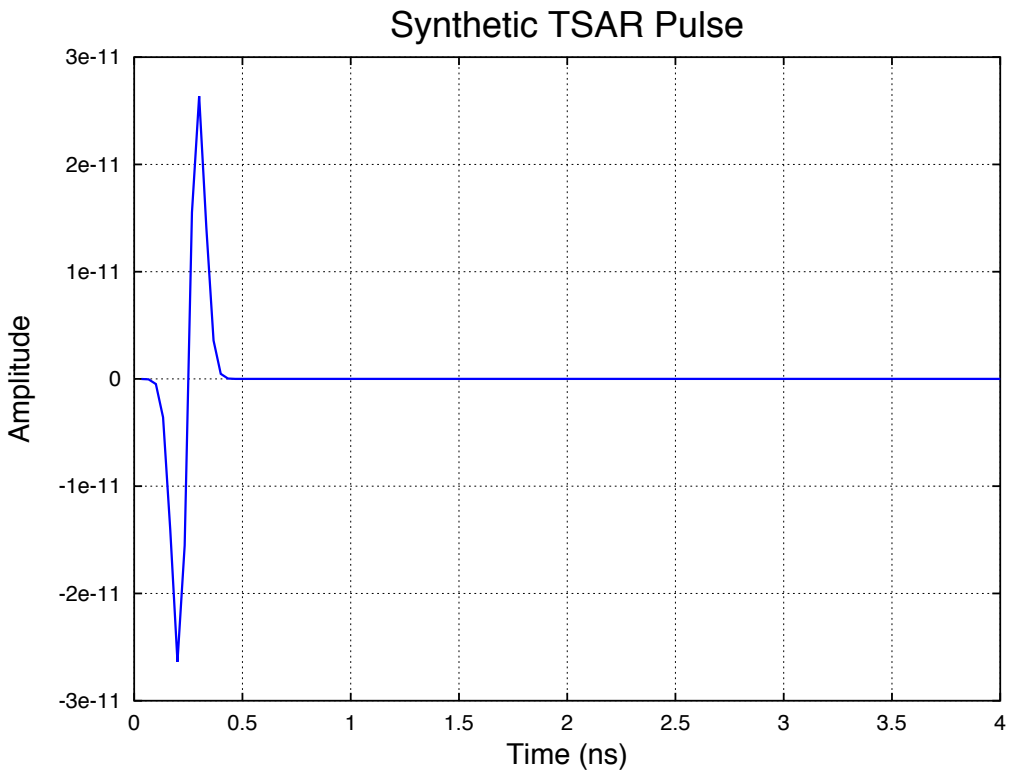

FIG. 9. Ultrawideband pulse used as input in simulation of the TSAR data. The analytic form of the pulse is given in equation 4.

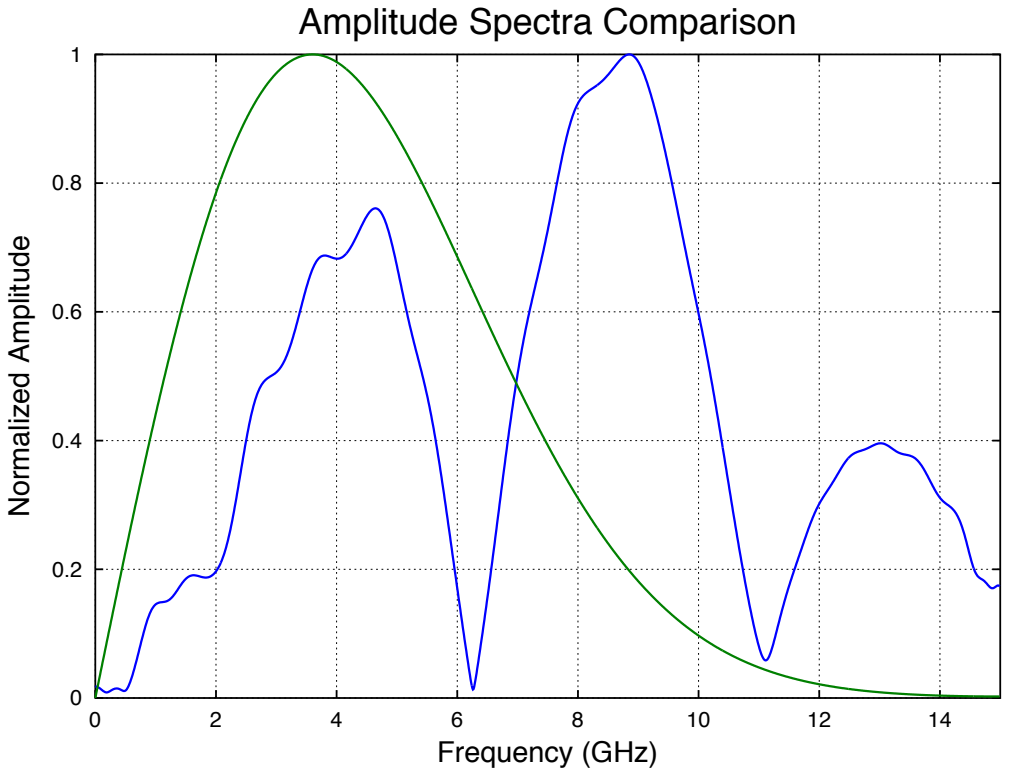

FIG. 10. Comparison of amplitude spectra of trace 35 of the TSAR data *blue* and synthetic TSAR pulse *green*, (Figure 9). The amplitude spectra of the pulse was used to filter out the noisy parts of the data spectrum above ≈ 8 GHz, corresponding to instrument noise.

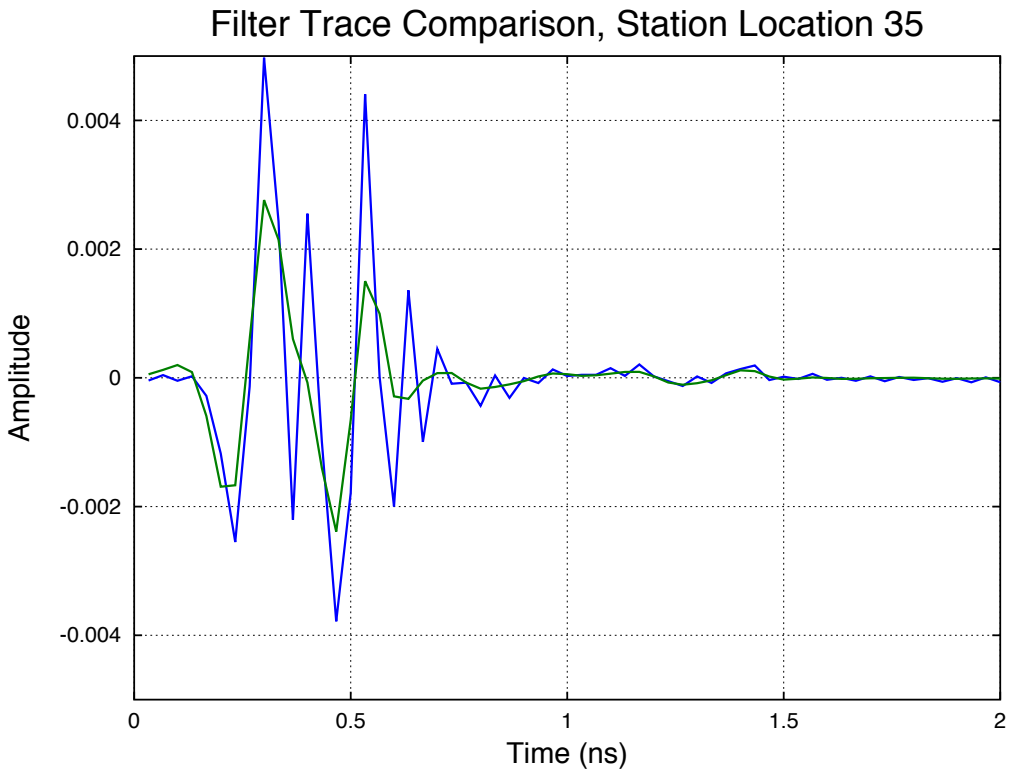

FIG. 11. Comparison of a TSAR data trace before and after weighting by the spectra of the TSAR pulse.

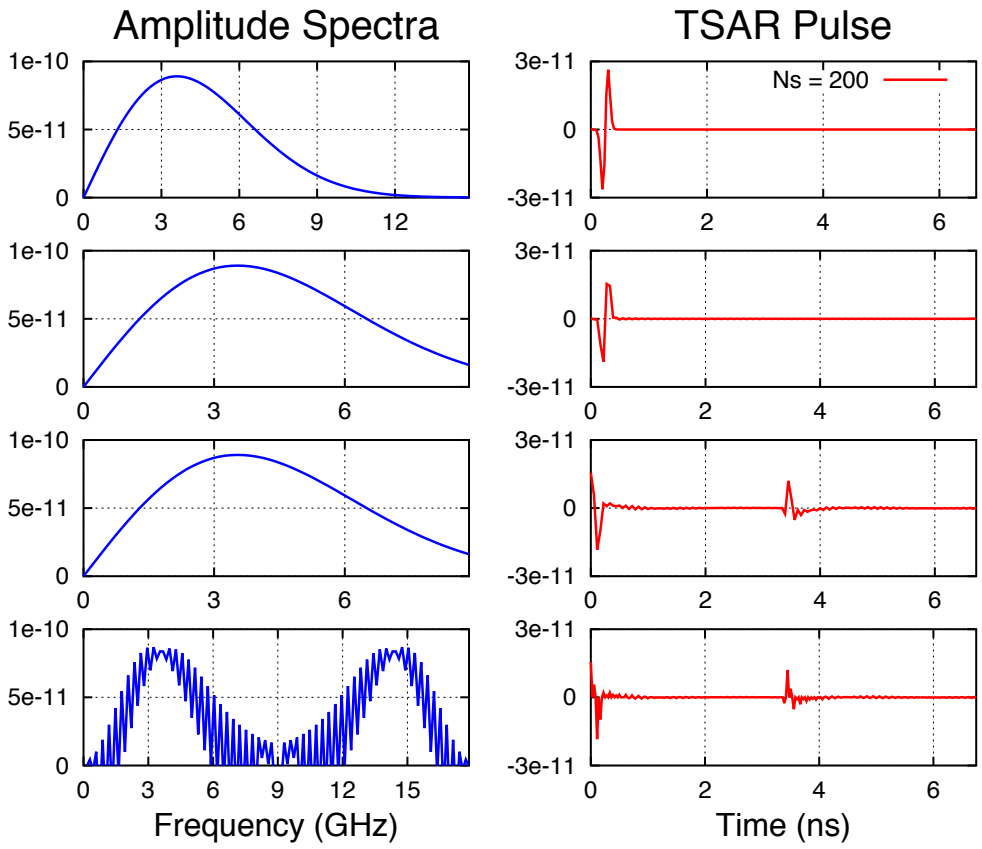

FIG. 12. Estimation of minimum phase equivalent of the TSAR pulse using the method described in Lamoureux and Margrave (2007b). THe input TSAR pulse and spectrum are in the top row. The second row contains the amplitude spectrum truncated to 9 GHz and the resultant TSAR time signal. The third row contains the minimum phase estimation as given by the MATLAB function *rceps* with its corresponding spectra, and the bottom row gives the result of upsampling by inserting a 0 between each datapoint.

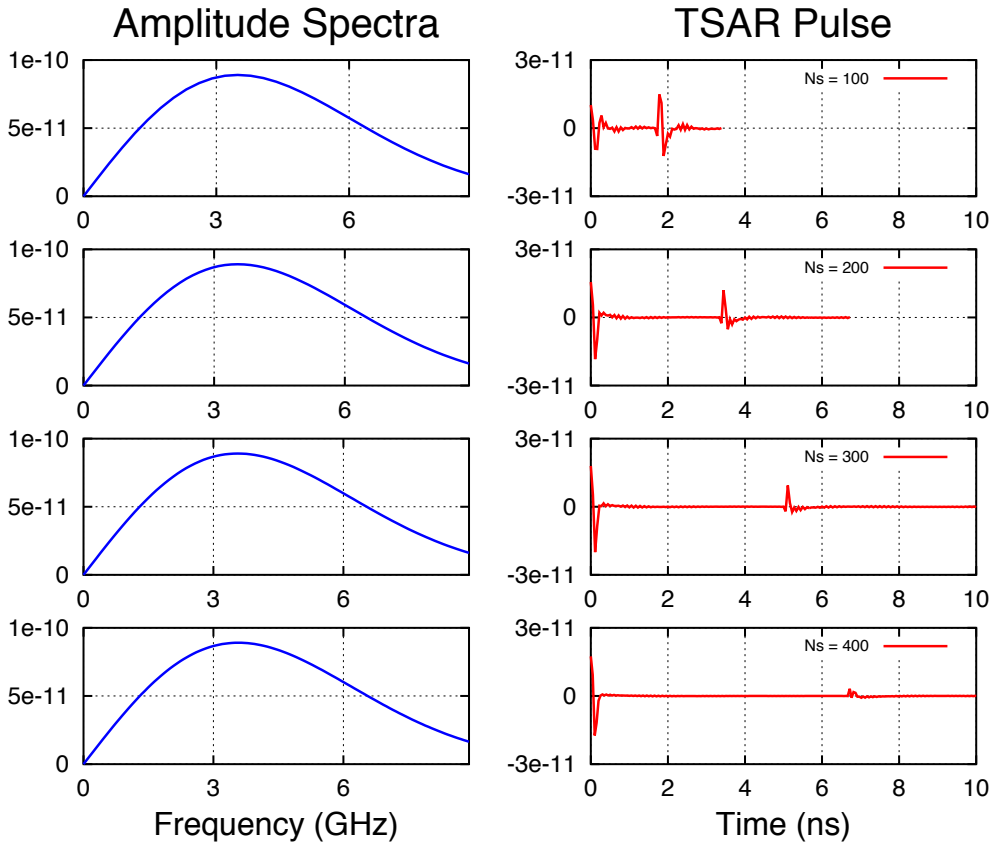

FIG. 13. Illustration of the different results obtained from the *rceps* function as a function of number of time samples in the input TSAR trace. The rows in this figure each translate to the third row in 12.

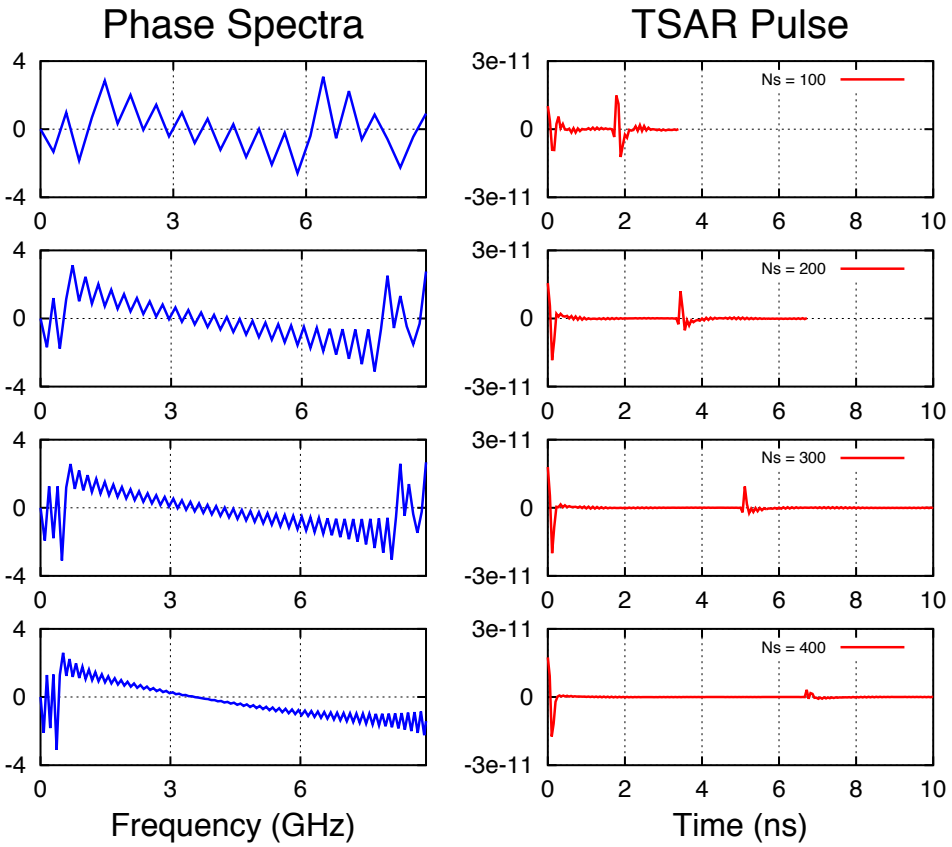

FIG. 14. Illustration of different phase spectra obtained from the *rceps* function as a function of number of time samples in the input TSAR trace. The rows in this figure each translate to the third row in 12, showing the phase spectra in the left column as opposed to the amplitude spectra.